Harper, P. W., & Hallett, S. R. (2010). A fatigue degradation law for cohesive interface elements - Development and application to composite materials. International Journal of Fatigue, 32(11), 1774-1787. 10.1016/j.ijfatigue.2010.04.006

Published in International Journal of Fatigue 2010, 32(11), Pages 1774–1787
DOI: 10.1016/j.ijfatigue.2010.04.006

# A FATIGUE DEGRADATION LAW FOR COHESIVE INTERFACE ELEMENTS – DEVELOPMENT AND APPLICATION TO COMPOSITE MATERIALS

**Paul W. Harper and Stephen R. Hallett**

University of Bristol

Advanced Composites Centre for Innovation and Science

Queen's Building, University Walk, Bristol, BS8 1TR, UK

Email: paul.harper@bris.ac.uk

**Keywords:** Cohesive Zone, Delamination, Interface Elements, Fatigue

**Abstract:**

A cohesive zone interface element degradation law is presented for analyzing delamination crack propagation under cyclic loading. Development of the law is based on a detailed study of the numerical cohesive zone and the extraction of strain energy release rate from this zone, enabling a direct link with experimental Paris Law data. The law is implemented using three dimensional interface elements within the explicit finite element code LS-Dyna. Validation is presented by way of application to composite material fatigue fracture toughness tests; Double Cantilever Beam for Mode I, End Notch Flexure for mode II and Mixed Mode Bending for the mixed mode case. In all cases good agreement with experimental data available in the open literature and/or theoretical solutions was obtained.

Published in International Journal of Fatigue 2010, 32(11), Pages 1774–1787
DOI: 10.1016/j.ijfatigue.2010.04.006

**Nomenclature**

**Interface Element Properties:**

| | |
|---|---|
| $G_C$ | Critical Strain Energy Release Rate |
| $K$ | Interface Element Stiffness prior to damage initiation |
| $\sigma$ | Interface Element Stress |
| $\sigma_{max}$ | Maximum Interfacial Stress |
| $\delta$ | Interface Element Relative Displacement |
| $\delta_e$ | Interface Element Relative Displacement at damage initiation |
| $\delta_f$ | Interface Element Relative Displacement at final failure |

Additional subscripts *I*, *II* and *m* are used to denote properties under mode I, mode II and mixed mode loading.

**Material Properties:**

| | |
|---|---|
| $E_{11}, E_{22}, E_{33}$ | Young's Moduli (subscripts 1, 2 and 3 denote the principal material axes) |
| $G_{12}, G_{13}, G_{23}$ | Shear Moduli |
| $\nu_{12}, \nu_{13}, \nu_{23}$ | Poisson's Ratios |

**Geometric Properties:**

| | |
|---|---|
| $a$ | Crack Length |
| $B$ | Laminate Width |
| $h$ | Laminate Half Thickness |
| $I$ | Second Moment of Area |

**Miscellaneous:**

| | |
|---|---|
| $C$ | Paris Law Constant |
| $m$ | Paris Law Exponent |
| $D_{tot}$ | Damage parameter, consisting of both quasi-static and fatigue damage |
| $d_s$ | Quasi-static damage parameter |
| $d_f$ | Fatigue damage parameter |
| $G_T$ | Total Strain Energy Release Rate (subscripts I/II used to denote mode I/II components) |
| $G_{max}$ | Maximum Strain Energy Release Rate in each fatigue cycle |
| $L_{CZ}$ | Numerical Cohesive Zone Length |
| $L_{CZ,f}$ | Fully Developed Numerical Cohesive Zone Length in a quasi-static analysis |
| $L_D$ | Fatigue crack length across an individual element |
| $L_{el}$ | Element Length |
| $L_{fat}$ | Fatigue Damage Zone Length |
| $L_{qs}$ | Quasi-static Damage Zone Length |
| $N$ | Number of fatigue cycles |
| $N_{el}$ | Number of elements within the numerical cohesive zone |
| $P$ | Load |
| $t$ | Time |
| $\Delta$ | Cantilever Tip Displacement |

Published in International Journal of Fatigue 2010, 32(11), Pages 1774–1787
DOI: 10.1016/j.ijfatigue.2010.04.006

## 1. Introduction

In finite element analysis, cohesive interface elements placed along potential crack propagation paths are becoming widely used for modelling interfacial failure. In laminated fibre reinforced composite materials failure between layers (or plies) is considered to be one of the most detrimental failure modes to occur since it occurs at relatively low loads and results in significant loss of structural properties [1]. Prediction of delamination failure is therefore of great interest to engineers designing composite structures. Interface elements are becoming widely used to predict such delamination failures [2,3,4,5,6,7]. They are also being successfully applied to predicting crack propagation along adhesive bond-lines [8,9,10,11].

An interface element is a special element that is placed along lines or planes of potential failure in a finite element model. Its behaviour is governed by a traction-displacement curve, in which stress generally increases from zero to the interface material's maximum stress ($\sigma_{max}$), before degrading back to zero, resulting in complete failure. Figure 1 shows the quasi-static response of a typical interface element formulation, governed by a bi-linear traction-displacement curve, applied to the Double Cantilever Beam (DCB) test for pure mode I fracture behaviour [12]. Behaviour under mode II and mixed mode loading is discussed in detail in section 3 of this paper. Although the shape of the interface element traction-displacement curve can take numerous forms, the total area enclosed must equal the critical fracture energy of the material ($G_C$) for an accurate delamination analysis to be gained under quasi-static loading.

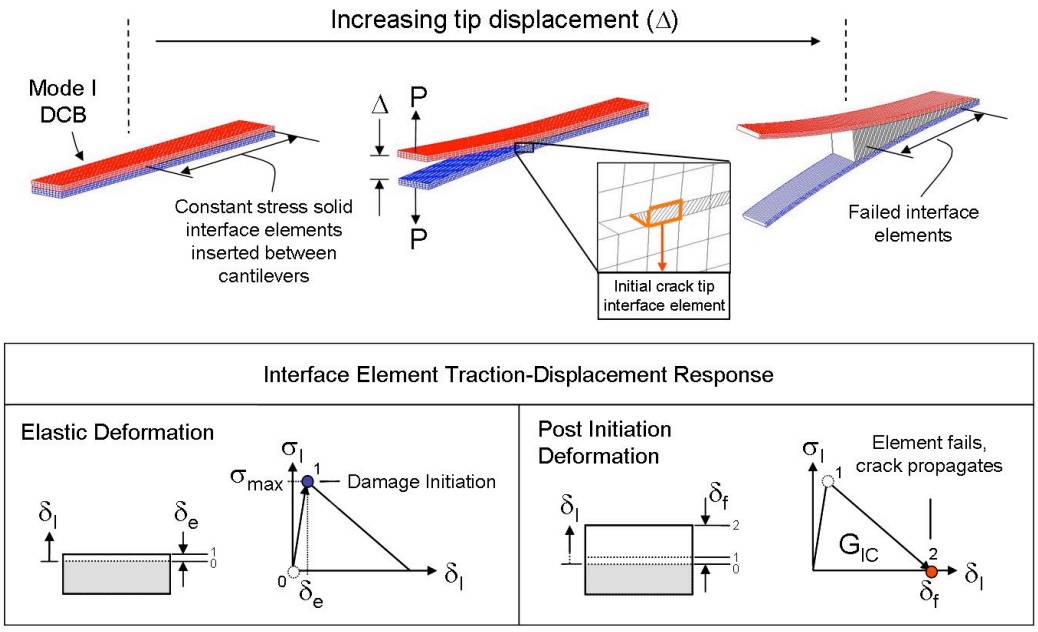


**Figure 1: The bi-linear traction-displacement curve**

Published in International Journal of Fatigue 2010, 32(11), Pages 1774–1787
DOI: 10.1016/j.ijfatigue.2010.04.006

Under fatigue loading, delamination growth from an initial defect can be represented using a Paris type curve, where the crack propagation rate is linearly related to strain energy release rate (or crack tip stress intensity factor) when plotted on a log-log scale [13,14], as shown in Figure 2. For design of composite structures this enables one of two approaches to be adopted:

i) A no-growth design philosophy, determined by ensuring the applied load does not result in the crack tip strain energy release rate reaching a value such that the crack will propagate.

ii) A damage tolerant design approach, where a crack is allowed to grow provided that it will not result in catastrophic failure between inspection intervals.

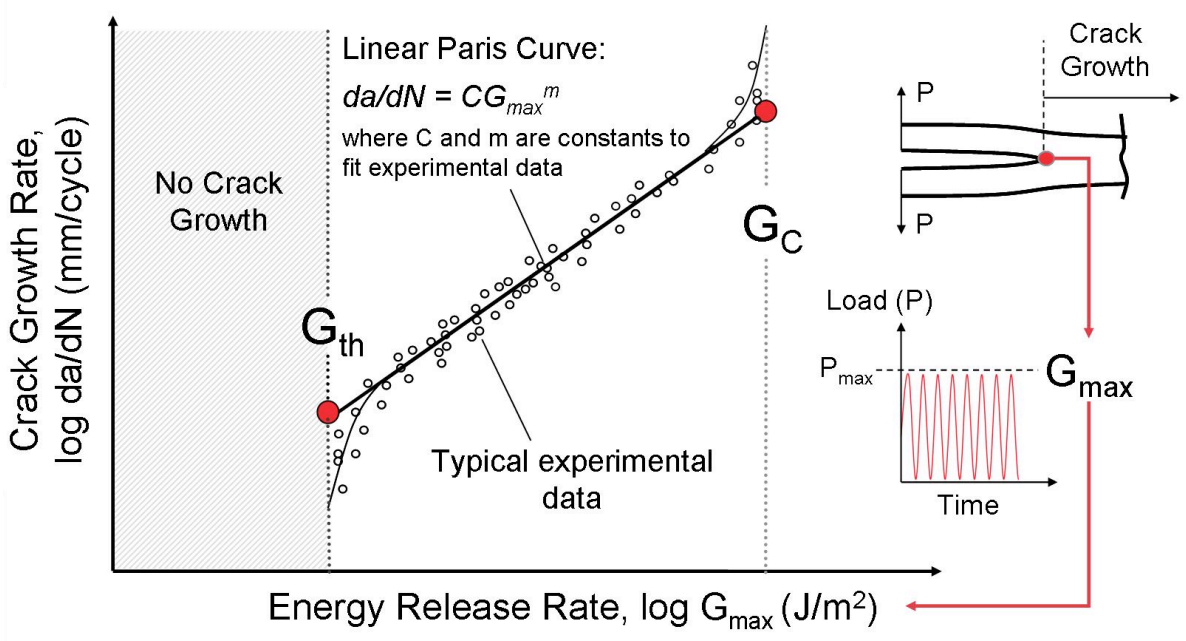


**Figure 2: The Paris Law Curve**

The Virtual Crack Closure Technique (VCCT) has previously been employed to extract crack tip strain energy release rate and hence analyse crack propagation using the Paris Law [15,16,17]. Such a technique requires complex algorithms to monitor the numerical crack tip and allow propagation by releasing constraints on duplicate nodes. For this reason, the expected path of propagation must be known in advance and the method has only gained widespread use in 2D numerical models with one or two crack fronts. In some cases, automated algorithms have been introduced to overcome such limitations [18,19]. Implementing a cohesive zone degradation law into interface elements provides an alternative method to overcome these limitations. Whilst formulations have been developed to account for damage under cyclic loading [20,21,22,23,24], these tend to

Published in International Journal of Fatigue 2010, 32(11), Pages 1774–1787
DOI: 10.1016/j.ijfatigue.2010.04.006

require calibration factors which do not directly link physical material properties to experimental results. Turon et al. [25,26] have recently attempted to improve this by developing a fatigue law which maintains a direct link between linear elastic fracture mechanics and the interface element damage algorithm. Although no standard test methods exist for fatigue crack propagation in composites, Turon's law uses parameters directly obtainable from fracture toughness specimens such as the Double Cantilever Beam (Mode I), End Notched Flexure (Mode II) and Mixed Mode Bending specimens, which have been widely used for gaining experimental Paris Law data for composite laminates [1,27,42]. The formulation also relies on analytical solutions for calculating the length of the non-linear cohesive zone which forms ahead of a crack tip. There has been some investigation on the general applicability of these solutions [28] and also improvements to original formulations proposed [29].

The current paper presents a new fatigue damage formulation that preserves the direct link with linear elastic fracture mechanics. It is based on strain energy release rate extraction from cohesive interface elements and demonstrates the necessity of a detailed understanding of the nature of the cohesive zone stress distribution. The law is implemented within the explicit finite element code, LS-Dyna, and results are presented for composite delamination models under mode I, mode II and mixed mode loading. As well as providing potential to simulate impact damage and subsequent fatigue crack propagation within a single coherent simulation, use of an explicit solver can also avoid convergence problems, often encountered in implicit analyses when modelling strongly non-linear events [4].

**2. Interface Element Constitutive Law**

The interface elements used for this research take the form of solid hexahedral elements with a small initial thickness, governed by a bi-linear constitutive law [30]. This was developed from a discrete interface element formulation, which was successfully implemented to model both matrix cracking and delamination within notched composites using the explicit finite element code 'LS-Dyna' [7]. Full details of the interface element constitutive behaviour under quasi-static loading, from which the fatigue formulations presented here were developed, are provided in references [7] and [30]. Only a brief recap of the important features of the quasi-static interface element model is therefore given here.

The formulation can be illustrated using a single three-dimensional map by representing the normal opening mode (mode I) on the $0$ - $\sigma$ - $\delta_{normal}$ plane, and the transverse shear mode on the $0$ - $\sigma$ - $\delta_{shear}$ plane, as shown in Figure 3. Mode II and mode III shear are not treated separately, instead the transverse shear component

Published in International Journal of Fatigue 2010, 32(11), Pages 1774–1787
DOI: 10.1016/j.ijfatigue.2010.04.006

is made up of the combined resultant shear, referred to as mode II within this paper for simplicity. The triangles $0$ - $\sigma_{I,max}$ - $\delta_{I,f}$ and $0$ - $\sigma_{II,max}$ - $\delta_{II,f}$ are the bi-linear responses in pure opening and pure shear respectively. Any point on the $0$ - $\delta_{normal}$ - $\delta_{shear}$ plane represents a mixed-mode relative displacement.

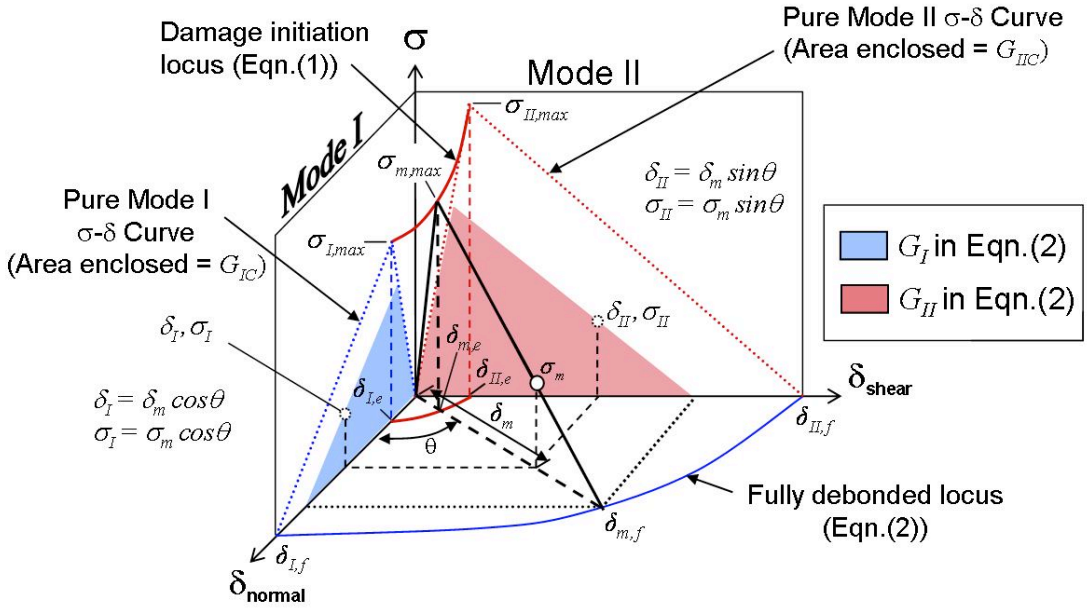


**Figure 3: The bi-linear traction-displacement response**

Under load, the interface relationship is initially elastic until reaching the damage onset displacement. For pure mode I or mode II loading, this elastic behaviour is governed by the mode I or mode II elastic stiffness, $E_I$ or $E_{II}$, until reaching the maximum mode I or mode II interfacial stress. Under mixed mode loading, the damage onset displacement, $\delta_{m,e}$, and maximum interfacial stress, $\sigma_{m,max}$, are calculated using a quadratic damage onset criterion, equation 1, which has been successfully used to predict mixed mode damage onset in previous investigations [31,32].

$$\sqrt{\left(\frac{max(\sigma_I, 0)}{\sigma_{I,max}}\right)^2 + \left(\frac{\sigma_{II}}{\sigma_{II,max}}\right)^2} = 1 \qquad \text{(Eqn. 1)}$$

When the interface element is further loaded, its stress is assumed to degrade linearly until complete failure. For pure mode I or mode II loading, the corresponding failure displacements, $\delta_{I,f}$ or $\delta_{II,f}$, are calculated using the pure mode I or mode II maximum interfacial stress, $\sigma_{I,max}$ or $\sigma_{II,max}$ and the mode I or mode II fracture toughness, $G_{IC}$ or $G_{IIC}$. Under mixed mode loading, the failure displacement corresponding to complete

Published in International Journal of Fatigue 2010, 32(11), Pages 1774–1787
DOI: 10.1016/j.ijfatigue.2010.04.006

decohesion is calculated using the following power law failure criterion, which allows the failure locus shown in Figure 3 to be determined:

$$\left(\frac{G_I}{G_{IC}}\right)^{\alpha} + \left(\frac{G_{II}}{G_{IIC}}\right)^{\alpha} = 1 \qquad \text{(Eqn. 2)}$$

where $\alpha \in (1.0 \sim 2.0)$ is an empirical parameter derived from mixed-mode tests, and $G_{IC}$ and $G_{IIC}$ are critical energy release rates for pure mode I (opening) and pure mode II (shear) respectively. Previous work [7] has shown that for IM7/8552 carbon-epoxy pre-preg material, a value of α = 1 gives a best fit to experimental data from [33]. Pinho et al [6] found a value of α =1.21 to give a best fit to experimental data for T300/913 carbon-epoxy prepreg and for data from Juntti et al. [34] for HTA/6376C carbon epoxy pre-preg a value of α =1.23 is appropriate. For the mixed mode study presented within this paper, a value of α = 1 has been used for simplicity.

Under quasi-static loading, a static damage parameter, $d_s$, is used to track the accumulation of irreversible damage, where:

$$d_s(\delta_m) = \frac{\delta_m - \delta_{m,e}}{\delta_{m,f} - \delta_{m,e}} \qquad \text{(Eqn. 3)}$$

Element failure occurs when $d_s$ reaches a value of unity. The introduction of an additional variable to account for fatigue damage and its interaction with the static damage variable is detailed in section 4.

**3. The Numerical Cohesive Zone**

At the crack tip, a region known as a cohesive zone forms in which interface elements have exceeded their linear-elastic range and experience irreversible deformation. Figure 4 illustrates the development of this zone, using the example of a mode I DCB subject to an increasing tip displacement.

Published in International Journal of Fatigue 2010, 32(11), Pages 1774–1787
DOI: 10.1016/j.ijfatigue.2010.04.006

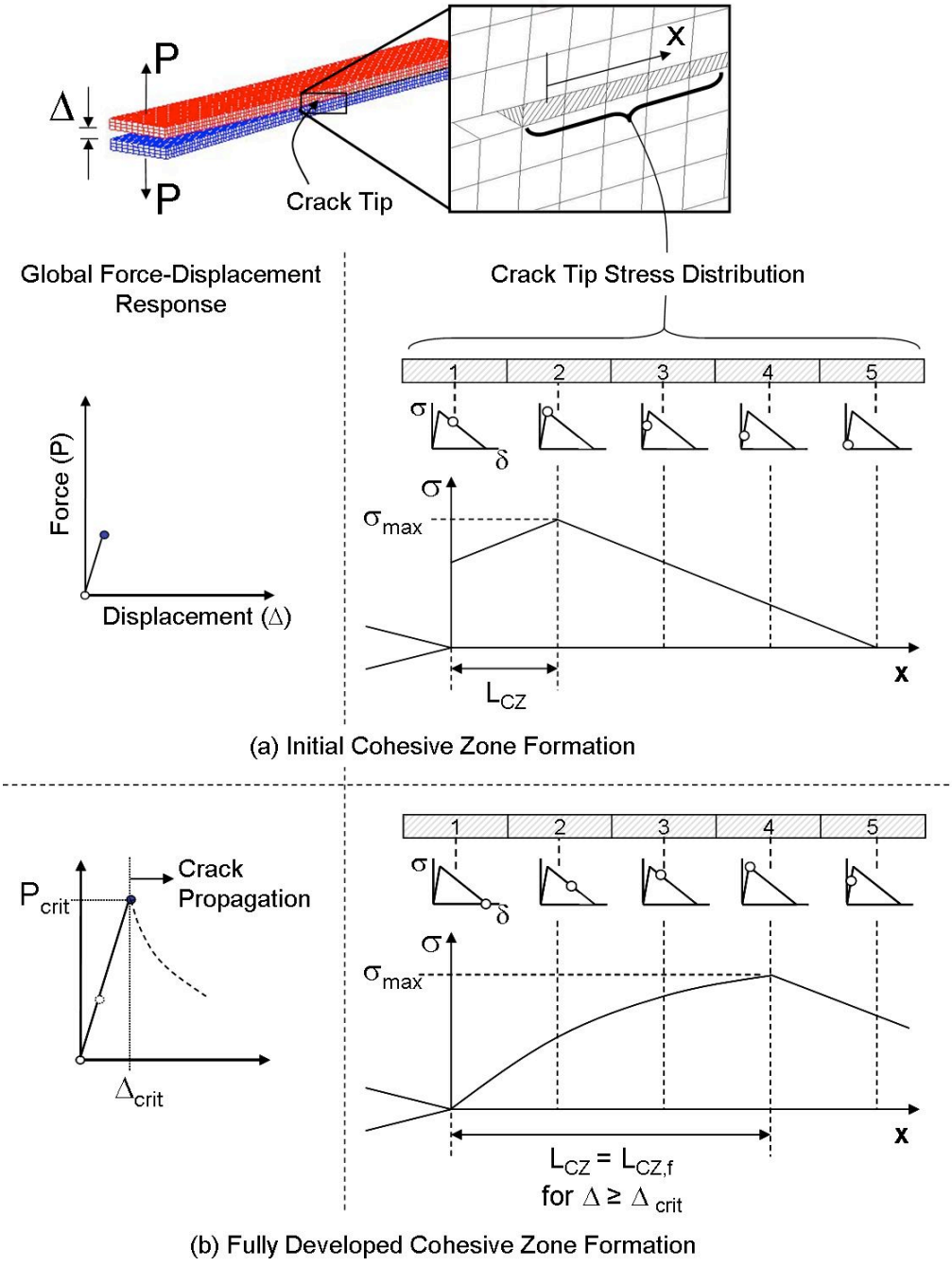


**Figure 4: Cohesive Zone Development in a mode I DCB**

As displacement initially increases, the interface element adjacent to the crack tip rapidly reaches its maximum interfacial stress and moves into the softening region of the traction-displacement response. As tip displacement increases further, element 2 also reaches its maximum stress and begins to experience irreversible deformation, allowing a cohesive zone to be defined. When the cohesive zone initially forms and spans only element 1 and element 2, the stress increase across the cohesive zone is shown as being linear due to the constant

Published in International Journal of Fatigue 2010, 32(11), Pages 1774–1787
DOI: 10.1016/j.ijfatigue.2010.04.006

stress within each interface element (i.e. due to the discretization of the cohesive zone it is not yet possible to determine the precise nature of stress variation across it). As loading continues, more interface elements experience irreversible deformation and the numerical cohesive zone reaches a fully developed length, $L_{CZ,f}$, at the point where the crack tip interface element (element 1) fails completely and the crack begins to propagate.

It is important to draw a clear distinction between the true physical cohesive zone length and the numerical cohesive zone length. For an accurate numerical representation of the physical cohesive zone, the shape of the traction-displacement curve must reflect the stress distribution associated with damage mechanisms occurring ahead of the physical crack tip [35]. However, for fibre reinforced composite materials, the length of the cohesive zone tends to be very short, typically of the order of 0.3-1mm [36] and, if only a global analysis of the structure's load-displacement response is required, results are relatively insensitive to the exact shape of the traction-displacement curve, provided that the correct maximum interfacial stress and fracture toughness are applied [37]. This explains why the bi-linear traction-displacement curve, which is geometrically the most simple form to implement, has become commonly used for delamination analyses [5,6,7]. Furthermore, once a crack has initiated in a structure and a cohesive zone exists, results are relatively insensitive to the exact value of maximum interfacial stress and only the fracture toughness value is of critical importance [28,38].

For quasi-static loading, it is necessary to ensure that sufficient elements exist within the cohesive zone for an accurate delamination analysis to be gained. This issue has been addressed at length in previous papers [28,38]. In developing a fatigue degradation law, which can be directly linked to Paris Law data, the following additional requirements apply:

1. Extraction of strain energy release rate from elements within the cohesive zone; this requires an understanding of how the stress distribution within the non-linear cohesive zone relates to the strain energy release rate from a linear elastic fracture mechanics analysis. This is essential in preserving a clear link with experimental Paris Law data, for which strain energy release rate is calculated based on the assumption of linear elasticity. It is important to note that for a high-cycle fatigue analysis, the applied load will be significantly less than that required for crack propagation in a quasi-static analysis, and prior to the fatigue degradation law being activated, the cohesive zone will only be partially developed.
2. Enabling the interface elements within the cohesive zone to be degraded such that the rate of crack advance matches that given by the Paris Law for the corresponding strain energy release rate and mode ratio.

Both of these require an understanding of the stress distribution and mode-ratio across the cohesive zone, and this has been investigated in [39]. It has been shown that a reasonable match to the strain energy release rate from a linear elastic fracture mechanics analysis can be obtained by integrating the traction-displacement response of an interface element directly adjacent to the crack tip. However, this requires a significantly finer mesh than that required purely to obtain an accurate load-displacement analysis, where only 2-3 interface elements are needed within the fully developed cohesive zone [28,38]. This is demonstrated in Figure 5, which compares strain energy release rate extraction with a global load-displacement analysis, for a mode I DCB using 3 different mesh densities. Whilst the coarsest mesh, which has 3 elements within the fully developed cohesive zone, can provide an accurate load-displacement analysis, only the finest mesh, which has 10 elements within the cohesive zone, can also provide a reasonable match to the analytical strain energy release rate. The corrected beam theory results shown have been calculated using a consistent method with that presented in reference [40]. This involves the application of correction terms to simple beam theory in order to account for shear deformation and local deformations that occur around the crack tip.

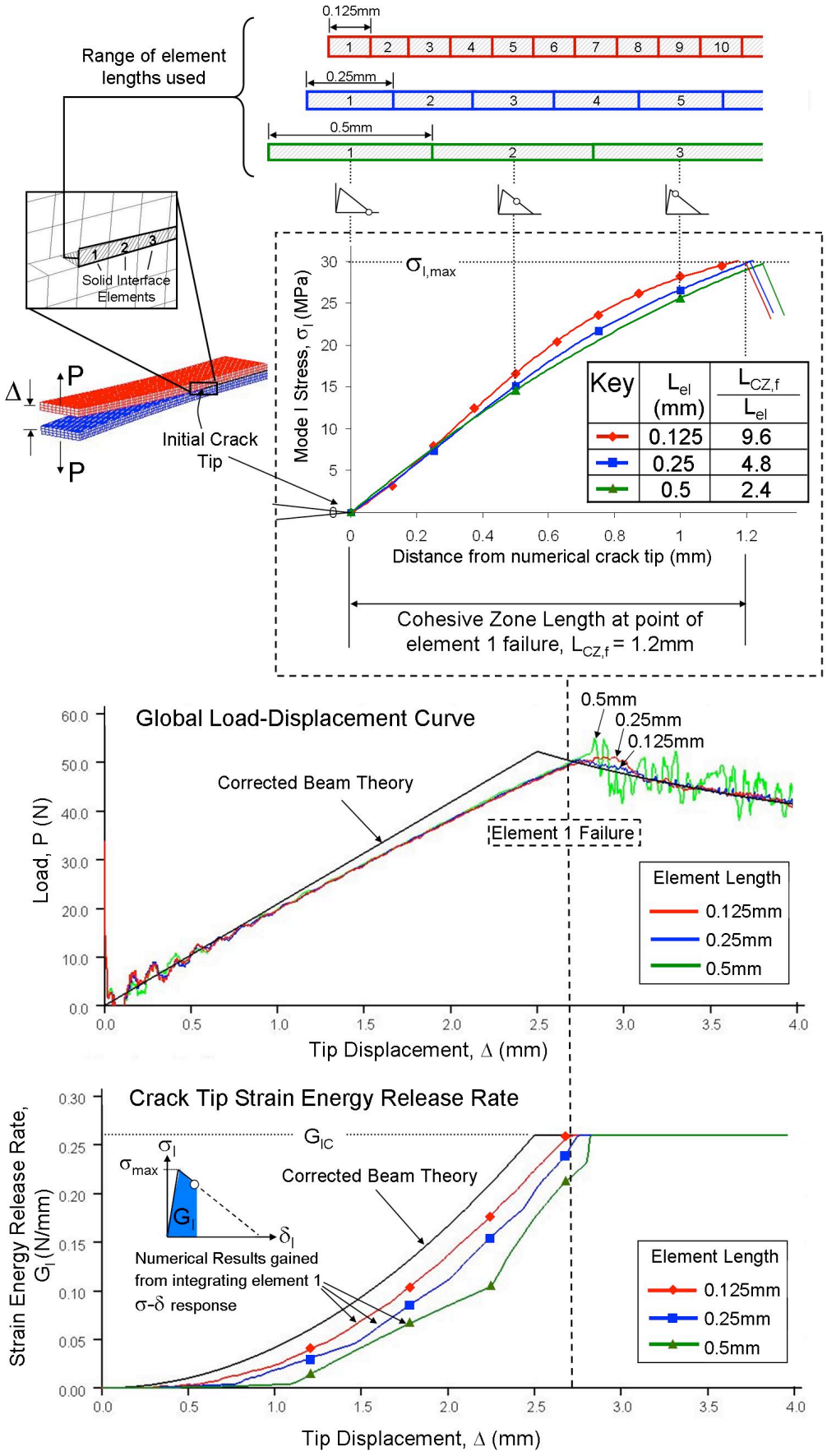


**Figure 5: Extraction of strain energy release rate**

Published in International Journal of Fatigue 2010, 32(11), Pages 1774–1787
DOI: 10.1016/j.ijfatigue.2010.04.006

**4. The Fatigue Damage Model**

There are two potential methods of modelling interface element damage accumulation under fatigue loading within a numerical code:

i) Tracking loading/unloading and degrading stiffness on a cycle-by-cycle basis [20,21,22,41]. Such an approach is likely to be the most beneficial for low-cycle fatigue applications in ductile materials, where there is potential for significant loading-unloading hysteresis, or where there are very frequent changes in the fatigue load amplitude. It is also likely to be the most suitable technique for including stick-slip effects in the model.

ii) Applying a loading envelope strategy, where the applied numerical load remains constant at the maximum value of the cyclic load being modelled, and the interface element is degraded based on a discrete number of elapsed cycles after each model time-step. Avoiding the need to explicitly model each individual fatigue cycle provides vastly greater computational efficiency and this approach is best suited to high-cycle fatigue applications, which may involve in excess of $10^6$ cycles, and tend to involve very small zones of irreversible deformation, particularly in brittle materials such as fibre reinforced composites.

Since the fatigue law presented in this paper has been developed for high-cycle fatigue applications, a cycle-jump strategy has been adopted due its greater computational efficiency. Fatigue is simulated by first applying a linearly increasing quasi-static load from zero to the maximum value that will occur in each fatigue cycle. Since it is an explicit analysis the load is then held constant for a period long enough to allow any residual dynamic effects to stabilise, although the loading rate is set such that these are minimised. Once equilibrium is achieved, the fatigue damage algorithm is activated. The applied numerical load then remains constant, but the fatigue law degrades the strength of interface elements based on the assumption of cyclic loading, relating "frequency" to the analysis time and allowing crack advance to occur (see Figure 6). The "frequency" referred to in the figure relates to the number of cycles experienced by the model, not the actual experimental loading frequency. The analysis time is much shorter than reality for computational efficiency. Although the example of a load controlled fatigue simulation is provided, it is important to highlight that the fatigue degradation law makes no assumption regarding load or displacement control. The rate of fatigue degradation is determined purely by the strain energy release rate extracted from interface elements within the cohesive zone regardless of the global boundary conditions applied to the model.

Published in International Journal of Fatigue 2010, 32(11), Pages 1774–1787
DOI: 10.1016/j.ijfatigue.2010.04.006

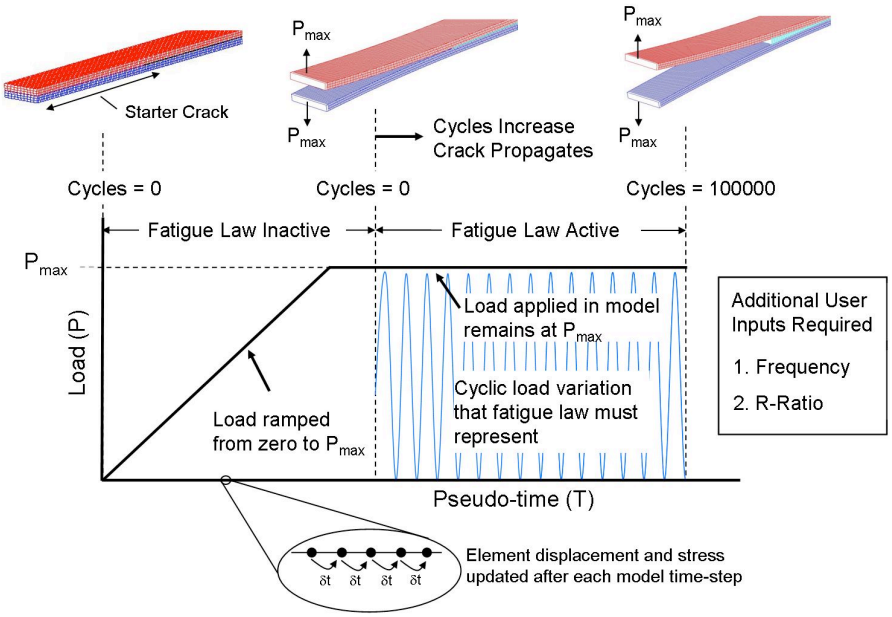


**Figure 6: Simulation of cyclic loading within LS-Dyna**

Since the applied numerical load remains constant, the user must supply the following model input parameters for cyclic loading to be accurately simulated:

i) Cycle frequency, $\partial N/\partial t$, expressed as cycles per second of LS-Dyna pseudo-time. This enables the crack propagation rate, $\partial a/\partial N$, expressed in terms of distance per cycle, to be converted to distance per unit of pseudo-time, $\partial a/\partial t$.

$$\frac{\partial a}{\partial t} = \frac{\partial a}{\partial N}\frac{\partial N}{\partial t} \qquad \text{(Eqn. 4)}$$

ii) R-Ratio, defined as the ratio between the minimum and maximum load ($P_{min}/P_{max}$) within each fatigue cycle. Assuming tension-tension fatigue loading, this allows the maximum strain energy release rate in each fatigue cycle, $G_{max}$, to be converted to the change in strain energy release rate during each fatigue cycle, $\Delta G$, using equation (5). The conversion of $G_{max}$ to $\Delta G$ is a requirement of the Paris Law model implemented for this study, as described in the following section.

$$\Delta G = G_{max}\,(1 - R^2) \qquad \text{(Eqn. 5)}$$

Immediately prior to the fatigue law being activated, the cohesive zone will be partially developed and due to the applied load remaining constant, the maximum strain energy release rate in each fatigue cycle, $G_{max}$, can be extracted from the integrated traction-displacement response of the interface element directly adjacent to the numerical crack tip (see Figure 5). Although the example shown is a pure mode I case, for a mixed mode load

Published in International Journal of Fatigue 2010, 32(11), Pages 1774–1787
DOI: 10.1016/j.ijfatigue.2010.04.006

case, the separate mode I and mode II components of strain energy release rate can be extracted using the relative mode I and mode II displacements of the traction-displacement response [39]. An appropriate Paris Law model can now be used to calculate the required rate of crack propagation, $\partial a/\partial N$. For the studies presented here, a model developed by Blanco *et al.* [14] has been implemented. This allows for a non-monotonic variation in the Paris Law co-efficients, $C$ and $m$, which experimental evidence has revealed to be the case for the HTA6376/C material modelled in this study [14, 42].

It is important to highlight that the mixed mode Paris Law model implemented in the analysis is purely a means of calculating the required crack growth rate under mixed mode load conditions by interpolating between a limited set of experimental input data. Blanco's model requires experimental Paris Law data under pure mode I, pure mode II and one mixed-mode load condition. However, many forms of mixed mode interpolation laws exist, as discussed at length in reference [14], and because the law implemented is a discrete component of the model, it can be easily varied to one most suitable for the material under investigation. The unique feature of the interface element fatigue degradation law is the direct extraction of strain energy release rate and mode-ratio from interface elements within the cohesive zone, which can be used in conjunction with any Paris Law model to calculate a rate of interface element degradation under mixed mode conditions and enable crack advance to occur.

Using Blanco's model, the rate of crack propagation is expressed in the form,

$$\frac{\partial a}{\partial N} = C\Delta G^m \qquad \text{(Eqn. 6)}$$

and for a general mixed model load case, the coefficients $C$ and $m$ are calculated using the following formulae:

$$log\, C = log\, C_I + \left(\frac{G_{II}}{G_T}\right) log\, C_m + \left(\frac{G_{II}}{G_T}\right)^2 log\, \frac{C_{II}}{C_m C_I} \qquad \text{(Eqn. 7)}$$

$$m = m_I + m_m\left(\frac{G_{II}}{G_T}\right) + (m_{II} - m_I - m_m)\left(\frac{G_{II}}{G_T}\right)^2 \qquad \text{(Eqn. 8)}$$

where the coefficients $C_I$, $C_{II}$, $C_m$, $m_I$, $m_{II}$ and $m_m$ are obtained from experimental Paris Law data for mode I, mode II and one mixed mode fatigue test, using standard fracture toughness measurement procedures such as the DCB, 3 or 4 point ENF and mixed mode bending specimens respectively. $G_T$, $G_I$ and $G_{II}$ are the total, mode I and mode II strain energy release rates respectively and within the fatigue algorithm, these are obtained by

Published in International Journal of Fatigue 2010, 32(11), Pages 1774–1787
DOI: 10.1016/j.ijfatigue.2010.04.006

integrating the interface elements' traction-displacement response, as previously discussed. Reference [14] gives full details of how Blanco's mixed mode interpolation law was developed and demonstrates the application of equation (7) and equation (8).

A rate of strength degradation and consequent failure must now be applied to interface elements within the cohesive zone so that the required rate of crack advance is accurately simulated. For this to be achieved, a fatigue damage parameter, $d_f$, is used as a measure of crack advance across each interface element. This is added to the interface element's static damage parameter, $d_s$, giving a value for total damage accumulated, $D_{tot}$:

$$D_{tot} = d_s + d_f \qquad \text{(Eqn. 9)}$$

$D_{tot}$ is used to calculate the interface element stress, $\sigma_m$, after each model time-step, with element failure occurring when the total damage ($D_{tot}$) reaches unity:

$$\sigma_m = \sigma_{m,max}(1 - D_{tot}) \qquad \text{(Eqn. 10)}$$

As shown by Figure 7, with the fatigue law active, the traction-displacement response extracted from a single element in a typical DCB test deviates significantly from the bi-linear quasi-static response. Understanding the nature of this failure path and how it relates to the interface element's position within the cohesive zone is vital to the calculation of the fatigue damage rate.

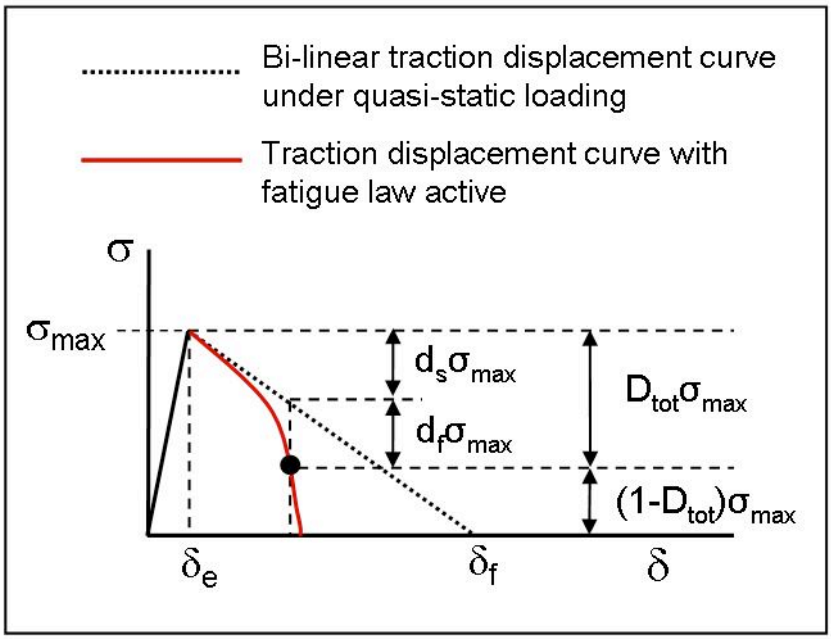


**Figure 7: Definition of the static and fatigue damage parameters**

Published in International Journal of Fatigue 2010, 32(11), Pages 1774–1787
DOI: 10.1016/j.ijfatigue.2010.04.006

In order to avoid the need for a crack path following algorithm, which would introduce significant computational expense, the rate of element failure within a fatigue simulation must account for the length and stress distribution of the cohesive zone. This is necessary because there is no easy means of detecting the position in relation to the numerical crack tip for interface elements within the cohesive zone. All of the elements throughout the entire cohesive zone are therefore acted on by the fatigue damage algorithm as soon as their strain energy release rate exceeds the threshold value. The algorithm acts to degrade the strength of elements within the cohesive zone, based on the strain energy release rate extracted, by integrating their traction-displacement response. Interface elements close to the numerical crack tip have the highest strain energy release rate and consequently, the highest rate of strength degradation when the fatigue law is activated. Interface elements further away from the crack tip have a lower strain energy release rate and a lower rate of strength degradation. Consequently, the traction-displacement response of interface elements close to the crack tip is found to exhibit an almost vertical gradient, with little further increase in displacement before failure. Interface elements further away from the crack tip, which have just entered the cohesive zone, initially follow a traction-displacement response which closely matches the bi-linear failure curve for pure quasi-static loading. As the interface elements ahead of them fail and they near the crack tip, their strain energy release rate and rate of strength degradation increase. Consequently, the gradient of their traction-displacement response also increases until reaching a near vertical state close to the crack tip.

These effects are illustrated in the top left hand diagram of Figure 8, labelled ‘actual response’ with the position of each interface element on the traction displacement curve being noted by its number (order from the crack tip). Although in reality each interface element’s failure path exhibits a curved response, the model assumes that it can be idealised as consisting of two linear regions (see Figure 8):

i) A quasi-static damage length, $L_{qs}$, in which elements are acquiring predominantly quasi-static damage and the integrated strain energy release rate is below the analytical crack tip value. The traction-displacement response in this region is assumed to be perfectly linear but at a slight angle to the pure quasi-static response due to the acquisition of some initial fatigue damage.

ii) A fatigue damage length, $L_{fat}$, in which elements are acquiring only fatigue damage and the integrated strain energy release rate is equal to the analytical crack tip value. The traction-displacement response in this region is assumed to be vertical.

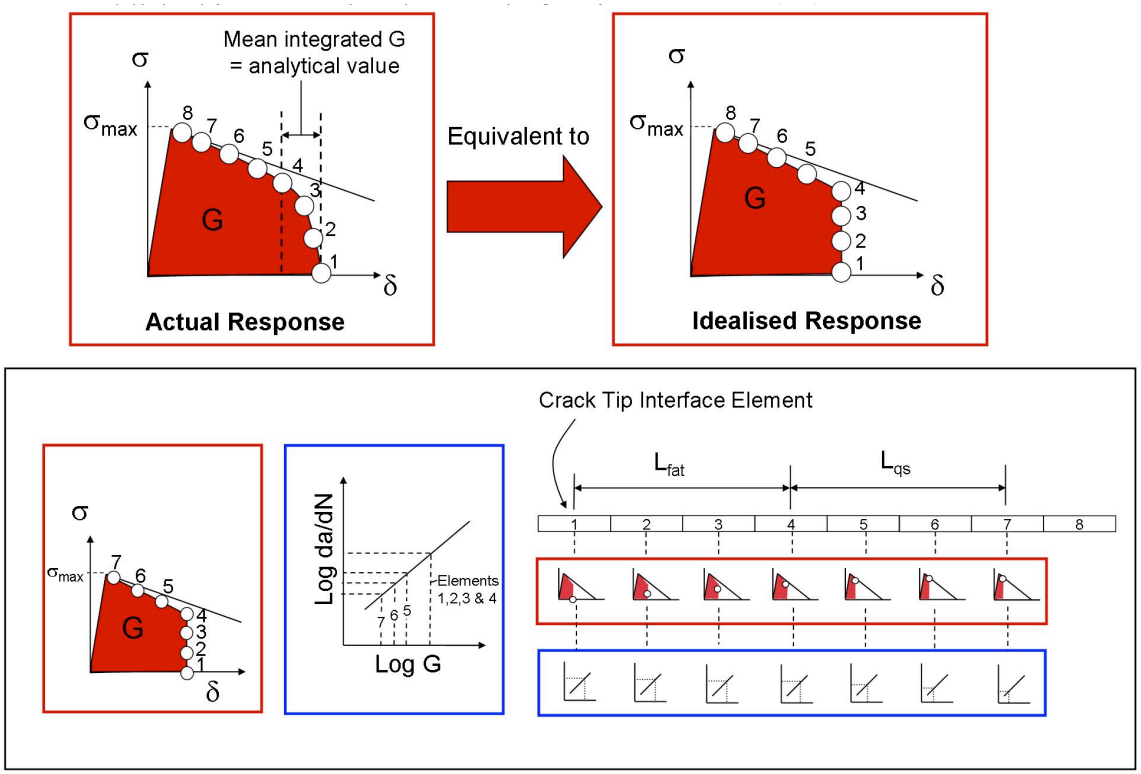


**Figure 8: Equivalent model showing quasi-static and fatigue damage lengths**

Since each interface element has no knowledge of its position within the cohesive zone, the accumulation of some fatigue damage in the quasi-static region cannot be prevented. It is thus necessary to account for this 'unwanted fatigue damage,' $d_{f,u}$, so that further fatigue damage can be applied at the correct rate when the element enters the fatigue damage zone. This is achieved by subtracting the integrated area under the actual traction-displacement response from the traction-displacement response assuming no fatigue damage (pure bi-linear response), as shown in Figure 9. By approximating the resultant area as a triangle, the magnitude of unwanted fatigue damage can be calculated.

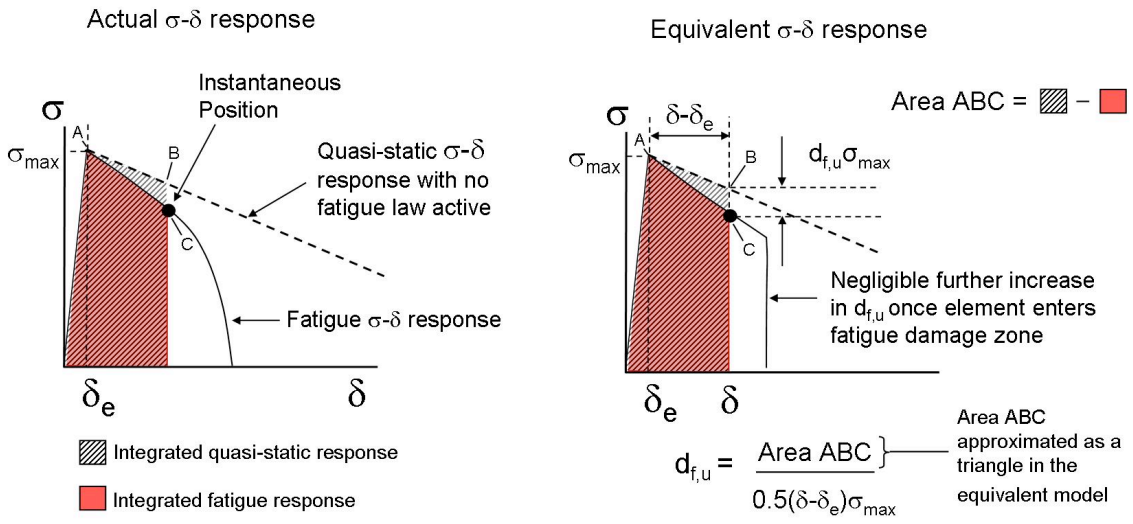


**Figure 9: Calculation of unwanted fatigue damage**

Published in International Journal of Fatigue 2010, 32(11), Pages 1774–1787
DOI: 10.1016/j.ijfatigue.2010.04.006

In order to account for the presence of unwanted fatigue damage, the assumed fatigue crack length across the element, $L_D$, is given by:

$$\frac{L_D}{L_{el}} = \frac{d_f - d_{f,u}}{1 - d_s - d_{f,u}} \qquad \text{(Eqn. 11)}$$

As shown by Figure 10, this is consistent with the element having no fatigue crack at the point of entry to the fatigue damage zone.

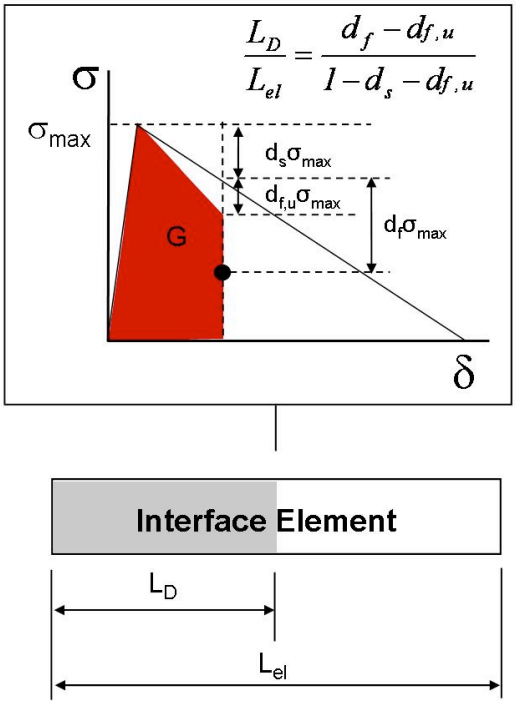


**Figure 10: Definition of interface element crack length, accounting for unwanted fatigue damage**

The additional new crack length is assumed to be equal to the sum of the crack lengths of all elements within the fatigue damage zone:

$$a = \sum_{e \in L_{fat}} L_D \qquad \text{(Eqn. 12)}$$

Therefore, the rate of crack advance is given by:

$$\frac{\partial a}{\partial N} = \sum_{e \in L_{fat}} \frac{\partial L_D}{\partial N} \qquad \text{(Eqn. 13)}$$

Since the rate of fatigue damage in each interface element, $\partial L_D/\partial N$, is calculated using the integrated strain energy release rate, assuming this is approximately equal for all elements within the fatigue damage length (a

Published in International Journal of Fatigue 2010, 32(11), Pages 1774–1787
DOI: 10.1016/j.ijfatigue.2010.04.006

reasonable assumption if the gradient of the traction-displacement response for elements within the fatigue damage length is close to vertical), the total rate of fatigue damage accumulation is given by:

$$\sum_{e \in L_{fat}} \frac{\partial L_D}{\partial N} = \frac{L_{fat}}{L_{el}} \frac{\partial L_D}{\partial N} \qquad \text{(Eqn. 14)}$$

As shown by equation (13), this total rate of fatigue damage accumulation is equivalent to the rate of crack advance, hence:

$$\frac{\partial a}{\partial N} = \frac{L_{fat}}{L_{el}} \frac{\partial L_D}{\partial N} \qquad \text{(Eqn. 15)}$$

We can now derive an expression for the required rate of increase of the fatigue damage parameter, $\partial d_f/\partial N$, in terms of the current position on the traction-displacement response, the length of the cohesive zone and the required rate of crack advance. We start by expressing $\partial d_f/\partial N$ in the following form:

$$\frac{\partial d_f}{\partial N} = \frac{\partial d_f}{\partial L_D} \frac{\partial L_D}{\partial N} \qquad \text{(Eqn. 16)}$$

We now use the previous equations to gain expressions for $\partial d_f/\partial L_D$ and $\partial L_D/\partial N$. Equation (11) can be differentiated and rearranged to provide the following expression for $\partial d_f/\partial L_D$:

$$\frac{\partial d_f}{\partial L_D} = \frac{1 - d_s - d_{f,u}}{L_{el}} \qquad \text{(Eqn. 17)}$$

Equation (15) can be rearranged to provide the following expression for $\partial L_D/\partial N$.

$$\frac{\partial L_D}{\partial N} = \frac{L_{el}}{L_{fat}} \frac{\partial a}{\partial N} \qquad \text{(Eqn. 18)}$$

Combining equations (16) (17) and (18) gives:

$$\frac{\partial d_f}{\partial N} = \frac{1 - d_s - d_{f,u}}{L_{fat}} \frac{\partial a}{\partial N} \qquad \text{(Eqn. 19)}$$

This shows that the rate of fatigue damage is not dependent on element length, but on the length of the fatigue damage zone in the direction of crack propagation. In order to calculate the fatigue damage zone length we need to know the fully developed cohesive zone length from a quasi-static analysis with no fatigue law active. As shown by previous studies [28,29], this is influenced by a range of material and geometric properties and there

are no existing analytical formulae which can accurately predict this. An important area of future work, both for this fatigue formulation and others involving cohesive zone length, will be to develop accurate predictive formulae for the numerical cohesive zone length in finite element models. The problem is currently resolved by performing a quasi-static analysis prior to activating the fatigue damage law and manually extracting the cohesive zone length. This length is then supplied as a user input to the fatigue damage algorithm. Although the cohesive zone length is subject to slight variation based on differences in mode-ratio and geometry as a crack advances, this does not significantly affect the accuracy of the analysis since we are considering only relatively small crack lengths with respect to the scale of the overall structure.

During a fatigue simulation, the length of the cohesive zone, comprising both the fatigue damage length and quasi-static damage length, is less than the fully developed cohesive zone length from a quasi-static analysis. Within the current formulation, it is estimated using the ratio between the integrated strain energy release rate, $G_T$, and the instantaneous critical fracture energy, $G_C$:

$$L_{CZ} = \frac{G_T}{G_C} L_{CZ,f} \qquad \text{(Eqn. 20)}$$

As will be demonstrated in later examples, it can generally be assumed that the quasi-static damage length and fatigue damage length each occupy half of this length. Hence, the fatigue damage length is calculated using:

$$L_{fat} = 0.5\left(\frac{G_T}{G_C}\right)L_{CZ,f} \qquad \text{(Eqn. 21)}$$

Combining this with equation (19) gives:

$$\frac{\partial d_f}{\partial N} = \frac{1 - d_s - d_{f,u}}{0.5\left(\frac{G_T}{G_C}\right)L_{CZ,f}} \frac{\partial a}{\partial N} \qquad \text{(Eqn. 22)}$$

where all of the parameters are either user inputs or are available from the interface element's traction-displacement response.

For each model time-step, the fatigue damage parameter is updated using:

$$d_{f,new} = d_{f,old} + \delta N \frac{\partial d_f}{\partial N} = d_{f,old} + f\delta t \frac{\partial d_f}{\partial N} \qquad \text{(Eqn. 23)}$$

where $f$ is the user-defined number of cycles per second of LS-Dyna pseudo-time,

Published in International Journal of Fatigue 2010, 32(11), Pages 1774–1787
DOI: 10.1016/j.ijfatigue.2010.04.006

$$f = \frac{\partial N}{\partial t} \qquad \text{(Eqn. 24)}$$

The main inputs and processes performed by the fatigue damage algorithm are summarized in Figure 11.

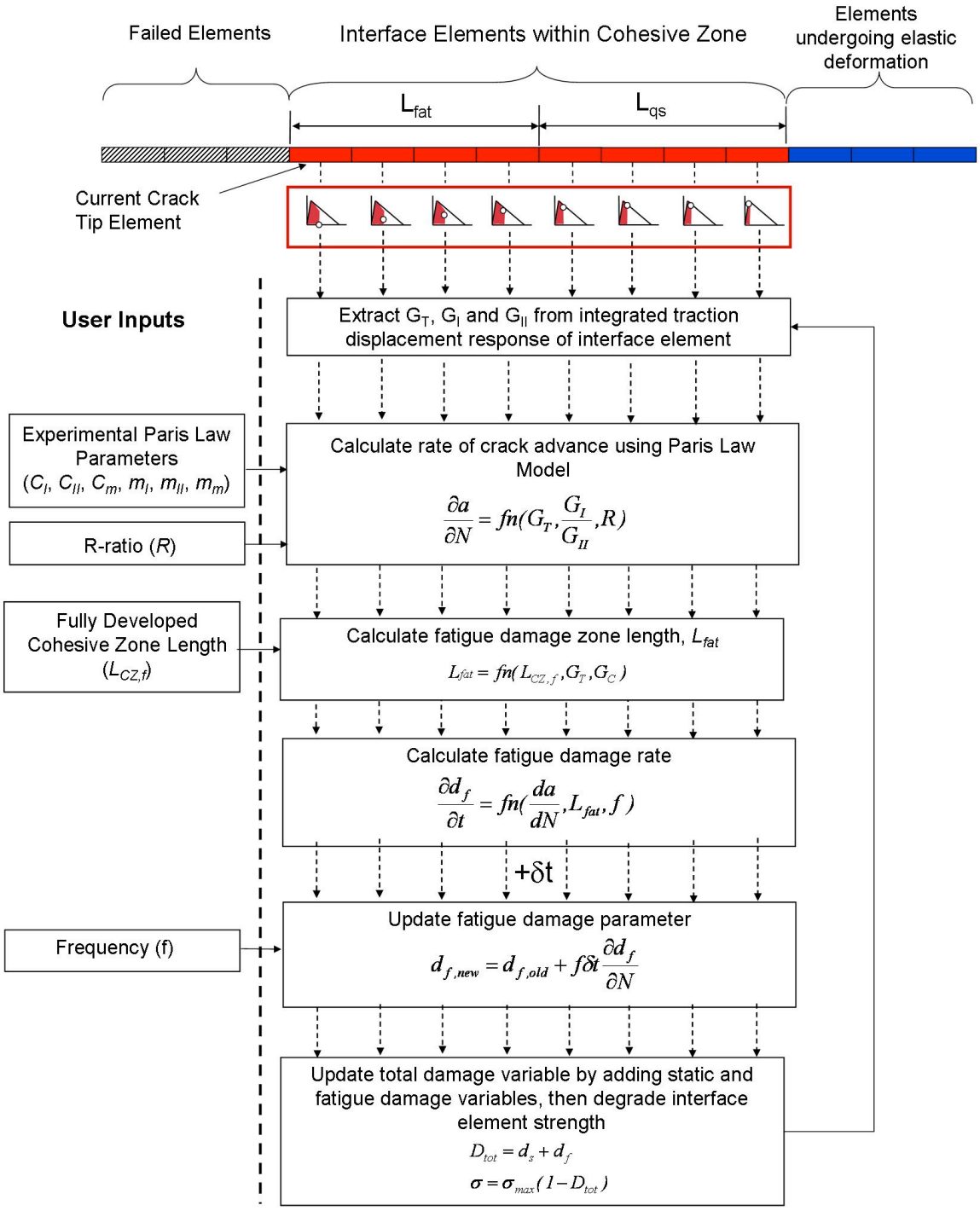


**Figure 11: The fatigue damage algorithm**

Published in International Journal of Fatigue 2010, 32(11), Pages 1774–1787
DOI: 10.1016/j.ijfatigue.2010.04.006

**5. Benchmark Models**

The fatigue algorithm has been validated under mode I, mode II and mixed mode loading using a DCB, 4 point End Notched Flexure (4ENF) and $G_I = G_{II}$ mixed mode model. The baseline specimen geometry, laminate properties and interfacial properties used for the numerical models are as shown in Figure 12 and Table 1. These are based on experiments on carbon fibre/epoxy HTA/6376C [14,42], which have been used by numerous researchers to validate numerical delamination analyses under both static [43] and fatigue loading [23,25]. All of the material properties listed in Table 1 are from reference [14] other than the mode I/II maximum interfacial stress and stiffness ($\sigma_{I,max}$,$\sigma_{II,max}$,$K_I$,$K_{II}$). Maximum interfacial stress has an extremely strong influence on cohesive zone length and the extremely short cohesive zone lengths resulting from the use of realistic interfacial strength values, has led to the use of reduced values in order to decrease the required mesh density [38]. For cases where an initial stress concentration or pre-crack exists, this has been shown to still allow an accurate delamination analysis provided that the cohesive zone length ahead of the crack tip does not become excessively long [28,38]. The values used for this investigation were chosen to provide a balance between ensuring that enough interface elements exist within the cohesive zone for accurate strain energy release rate extraction, whilst preventing excessively long cohesive zone lengths. The value of interfacial stiffness used provides an extremely stiff connection prior to damage initiation, whilst avoiding the numerical instabilities which can arise if this value becomes too high.

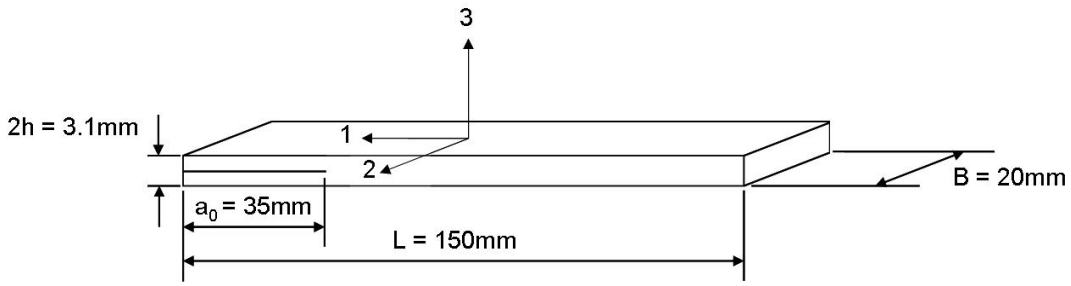


**Figure 12: Specimen Geometry**

Published in International Journal of Fatigue 2010, 32(11), Pages 1774–1787
DOI: 10.1016/j.ijfatigue.2010.04.006

**Table 1: Material Properties for HTA/6376C**

| **Laminate Properties** | | **Interfacial Properties** | |
|---|---|---|---|
| $E_{11}$ (MPa) | 120,000 | $G_{IC}$ (N/mm) | 0.26 |
| $E_{22} = E_{33}$ (MPa) | 10,500 | $G_{IIC}$ (N/mm) | 1.002 |
| $G_{12} = G_{13}$ (MPa) | 5,250 | $\sigma_{I,max}$ (MPa) | 30 |
| $G_{23}$ (GPa) | 3,480 | $\sigma_{II,max}$ (MPa) | 60 |
| $v_{12} = v_{13}$ | 0.3 | $K_I$ (N/mm$^3$) | $1\times10^5$ |
| $v_{23}$ | 0.51 | $K_{II}$ (N/mm$^3$) | $1\times10^5$ |
| **Fatigue Properties (Blanco's Paris Law model)** | | | |
| $C_I$ $(mm/cycle)(N/mm)^{-m}$ | 2.1 | $m_I$ | 5.09 |
| $C_{II}$ $(mm/cycle)(N/mm)^{-m}$ | 0.12 | $m_{II}$ | 4.38 |
| $C_m$ $(mm/cycle)(N/mm)^{-m}$ | 436,000 | $m_m$ | 5.48 |

Figure 13 shows details of the model setup and applied boundary conditions for each load case. Constant stress solid elements were used with one element across the specimen width and symmetry conditions applied along the specimen length. 3 elements were used through the thickness of each cantilever arm. Mass-scaling was applied to maintain a reasonable computational run time of a few hours and a global damping factor of 5 was applied to remove high frequency oscillations. Accurate results were maintained by ensuring that the kinetic and damping energy remained negligible compared to the strain energy absorbed by the specimen. For computational efficiency, details of the experimental rigs such as loading arms/rollers have not been included in the models, which is consistent with the approach adopted by other researchers when validating fatigue degradation laws [23,25]. Although this prevents accurate analysis of local stress concentrations around the loading points, global loads and displacements are not significantly affected. Therefore, conditions around the crack tip and the resulting strain energy release rate can still be accurately captured since the crack tip is always

Published in International Journal of Fatigue 2010, 32(11), Pages 1774–1787
DOI: 10.1016/j.ijfatigue.2010.04.006

a significant distance from the loading points. A frictionless contact surface was included to prevent penetration of the initial crack surfaces in the 4ENF test.

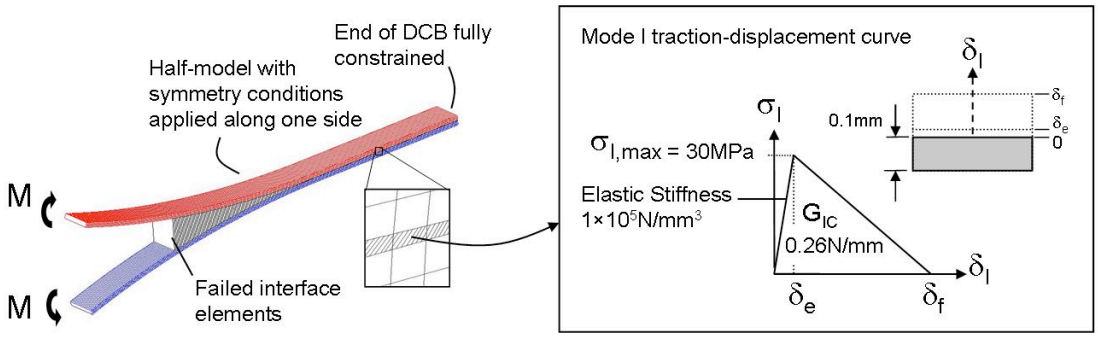


**(a) Mode I DCB**

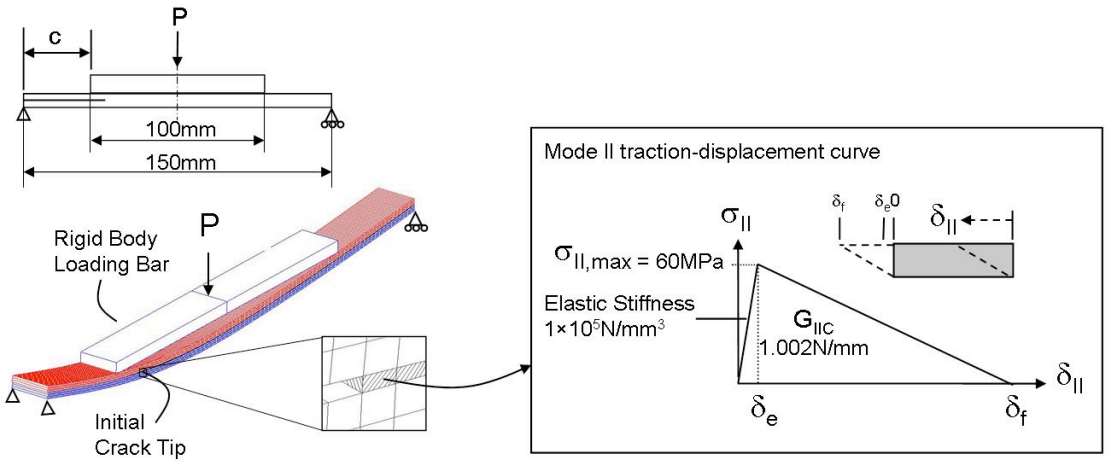


**(b) Mode II 4ENF**

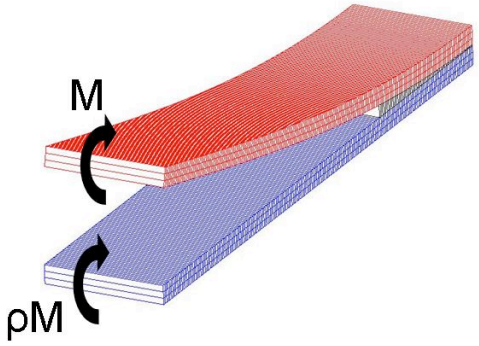


$$\rho = \frac{1-\frac{\sqrt{3}}{2}}{1+\frac{\sqrt{3}}{2}}$$

**(c) Mixed Mode Specimen (GI = GII)**

Published in International Journal of Fatigue 2010, 32(11), Pages 1774–1787
DOI: 10.1016/j.ijfatigue.2010.04.006

**Figure 13: Details of the numerical models and their applied boundary conditions**

Fatigue was simulated using the envelope loading approach described in the previous section and an R-ratio of 0.1 was maintained throughout. All of the specimens used for fatigue law validation allow load to be applied in a manner that maintains a constant analytical strain energy release rate with crack length. This eases the process of calculating the numerical crack propagation rate for each strain energy release rate and is consistent with the approach adopted by other researchers [23,25]. For the mode I DCB, this is achieved by applying a moment, $M$, to the cantilever tips, as shown in Figure 13 (a). Assuming linear elasticity, the analytical crack tip strain energy release rate, $G_I$, is given by:

$$G_I = \frac{M^2}{BEI} \qquad \text{(Eqn. 25)}$$

For the mode II 4ENF,

$$G_{II} = \frac{3P^2c^2}{16BEI} \qquad \text{(Eqn. 26)}$$

where $P$ and $c$ are the load and length defined in Figure 13 (b). For the mixed mode case, an identical model to the mode I DCB is used but moments of different magnitudes are applied to the two cantilever tips to achieve a mode-ratio of 50%, as shown in Figure 13 (c).

The strain energy release rates are given by:

$$G_I = G_{II} = \frac{3}{4\left(1+\frac{\sqrt{3}}{2}\right)^2}\frac{M^2}{BEI} \qquad \text{(Eqn. 27)}$$

The numerical crack propagation rate was calculated by recording the LS-Dyna pseudo-time taken for the crack to advance by 5mm. This was then converted to a distance per cycle value (mm/cycle) using the user defined relationship between fatigue cycles and pseudo-time. For each mode of loading, results were gained for at least 3 different strain energy release rates, enabling numerical Paris Law Curves to be generated. These were compared to the theoretical Paris Law curves generated when the analytical strain energy release rates are applied to Blanco's fatigue model. The experimental fatigue results from [42] used to obtain the Paris Law parameters supplied to the model have also been plotted for the pure mode I and mode II load cases.

Published in International Journal of Fatigue 2010, 32(11), Pages 1774–1787
DOI: 10.1016/j.ijfatigue.2010.04.006

**6. Results and Discussion**

Figure 14 shows results for the mode I DCB specimen using a constant element length of 0.125mm. To test the accuracy of the fatigue formulation for variations in interfacial properties and hence, different lengths of the cohesive zone, a mode I maximum interfacial stress of both 30MPa and 15MPa has been applied. As previously discussed, reducing the maximum interfacial stress increases cohesive zone length, and these values give fully developed cohesive zone lengths of 1.2mm and 2.4mm respectively (i.e. 9 and 19 interface elements within the fully developed cohesive zone). Close correlation exists between the theoretical Paris Curve and both sets of numerical results, indicating that the formulation is not significantly affected by the number of elements within the cohesive zone. Furthermore, interrogation of the cohesive zone with the fatigue law active supports the assumption of equal 'quasi-static damage zone' and 'fatigue damage zone' lengths for this mode case.

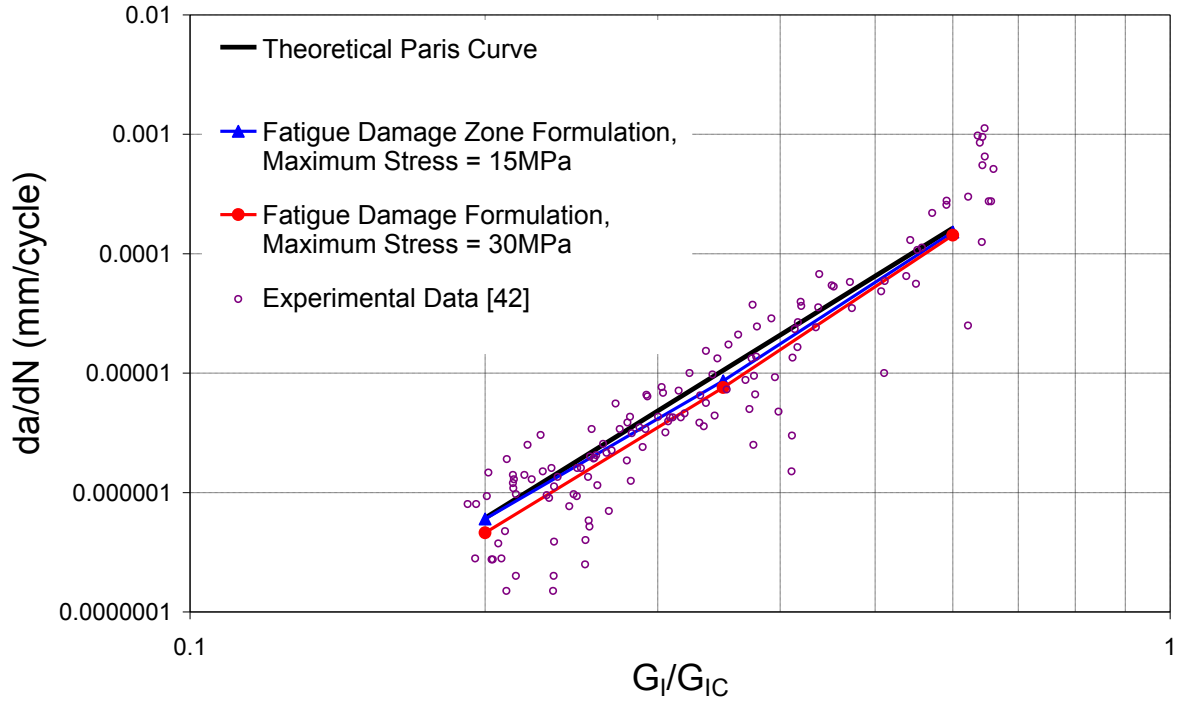


**Figure 14: Mode I fatigue results**

Figure 15 shows results for the mode II, 4 point ENF specimen. For this specimen, the maximum interfacial stress is maintained at its baseline value of 60MPa and the number of elements within the cohesive zone is varied by increasing the element length from 0.125mm to 0.25mm. This results in 32 and 16 elements respectively within the fully developed cohesive zone length of 4.1mm. Although numerical crack growth rates

Published in International Journal of Fatigue 2010, 32(11), Pages 1774–1787
DOI: 10.1016/j.ijfatigue.2010.04.006

for the two element lengths show close correlation, they are slightly lower than the theoretical Paris curve. Interrogation of elements in the cohesive zone with the fatigue law active suggested that the 'quasi-static damage zone' forms approximately 60% of the cohesive zone length for this particular case (i.e. a slight over-prediction of the 'fatigue damage zone' length results in an under-prediction of the crack growth rate). Future work will perform a more detailed investigation of the relative proportions of the cohesive zone occupied by the 'quasi-static damage zone' and 'fatigue damage zone' lengths for various mode-ratios.

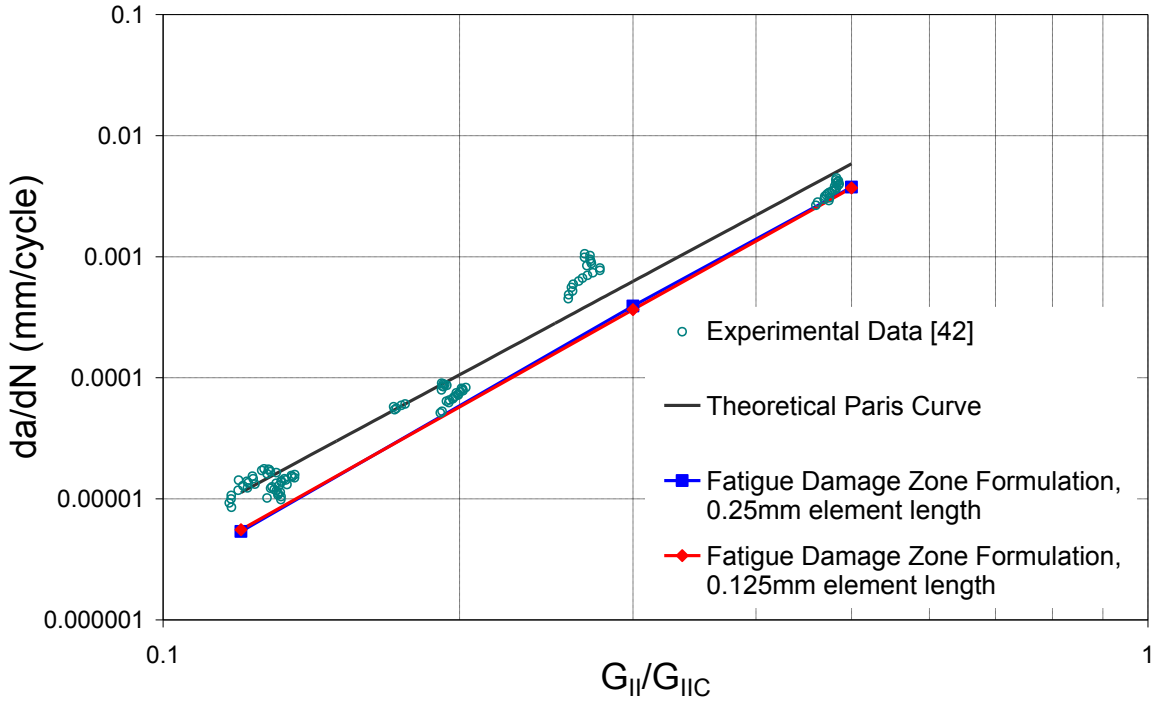


**Figure 15: Mode II 4ENF Results**

Figure 16 shows results for the mixed mode specimen using an element length of 0.125mm, which gives 12 elements within the specimen's fully developed cohesive zone length of 1.6mm. Although results show close agreement with the theoretical Paris Law curve, it was found that quite a significant variation in mode ratio occurs along the length of the cohesive zone, a feature also observed under pure quasi-static loading. This requires a more detailed investigation [39] in order to ensure that a direct link can be preserved between experimental Paris Law parameters, which are based on the assumption of linear elasticity at the crack tip, and values used to calibrate the fatigue law.

Published in International Journal of Fatigue 2010, 32(11), Pages 1774–1787
DOI: 10.1016/j.ijfatigue.2010.04.006

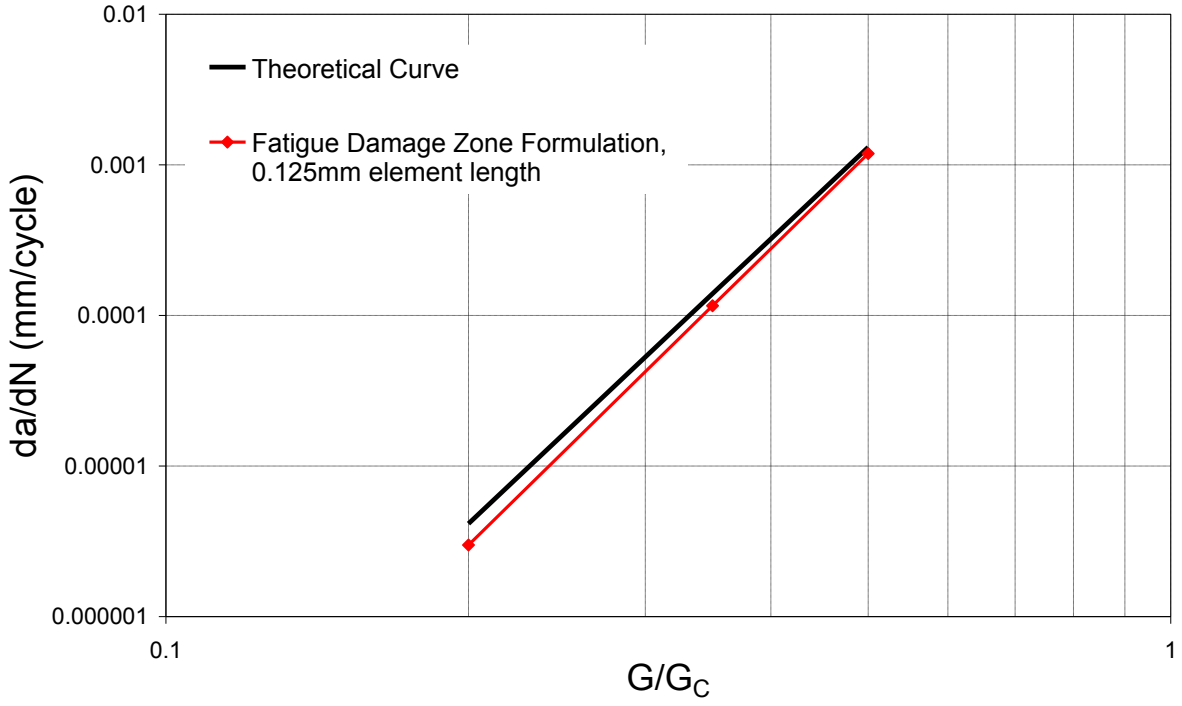


**Figure 16: Mixed Mode Results**

## 7. Conclusions

This study has presented a new formulation for predicting fatigue damage growth by relating the damage accumulation law of cohesive interface elements to Paris type crack growth laws. It has shown the importance of gaining a full understanding of the length and stress distribution of the cohesive zone in order to implement an accurate fatigue damage law, which requires no crack path following algorithm. This will become particularly advantageous as the models are applied to cases of increasing structural and geometric complexity. Such models may have numerous and curved crack fronts propagating simultaneously along several interfacial planes, for example, in ply drop features used to taper the thickness of composite structures such as helicopter rotor blades, wind/tidal turbines and aerospace engine fan blades. The damage formulation presented has addressed this need, whilst enabling a direct link to be maintained between experimental Paris Law parameters and model input parameters. Numerical results obtained from the fatigue model have shown good agreement with analytical crack propagation rates under mode I and mixed mode loading, whilst mode II, although less good is still quite reasonable. In addition, the model has been shown to be robust to variations in mesh density and material properties, both of which affect the number of interface elements within the cohesive zone.

A key feature of the formulation has been the division of the cohesive zone into two discrete regions, a 'quasi-static damage zone' and a 'fatigue damage zone,' which are currently assumed to be of equal length. Further investigation is required to more fully understand the traction-displacement failure response of interface elements in this zone and whether this assumption needs to be adjusted for different mode-ratios and cohesive zone lengths. Additionally, the technique could be improved by direct implementation of formulae to accurately predict the length of the numerical cohesive zone, but further work remains for these to be developed.

**References**

[1] R. Martin, Delamination Fatigue, in: B. Harris (Ed.), Fatigue in Composites, Woodhead Publishing Ltd, Cambridge, 2007, pp. 173-188.

[2] Z. Petrossian, M.R. Wisnom, Prediction of delamination initiation and growth from discontinuous plies using interface elements, Composites Part A: Applied Science and Manufacturing 29A (1998) 503-515.

[3] J. Chen, M. Crisfield, A.J. Kinloch, E.P. Busso, F.L. Matthews, Y. Qiu, Predicting Progressive Delamination of Composite Material Specimens via Interface Elements, Mechanics of Composite Materials and Structures 6 (1999) 301-317.

[4] M.A. Crisfield, G. Alfano, Finite element interface models for the delamination analysis of laminated composites: mechanical and computational issues, International journal for numerical methods in engineering 50 (2000) 1701-1736.

[5] P.P. Camanho, C.G. Davila, M.F. De Moura, Numerical Simulation of Mixed-mode Progressive Delamination in Composite Materials, Journal of Composite Materials 37 (2003) 1415-1424.

[6] S.T. Pinho, L. Ianucci, P. Robinson, Formulation and implementation of decohesion elements in an explicit finite element code, Composites Part A: Applied Science and Manufacturing 37 (2006) 778-789.

[7] W.G. Jiang, S.R. Hallett, B.G. Green, M.R. Wisnom, A concise interface constitutive law for analysis of delamination and splitting in composite materials and its application to scaled notched tensile specimens, International journal for numerical methods in engineering 69 (2007) 1982-1995.

Published in International Journal of Fatigue 2010, 32(11), Pages 1774–1787
DOI: 10.1016/j.ijfatigue.2010.04.006

[8] P.P. Camanho, C.G. Davila, S.T. Pinho, Fracture Analysis of Composite Co-cured Structural Joints Using Decohesion Elements, Fatigue & Fracture of Engineering Materials & Structures 27 (2003) 745-757.

[9] B.R.K. Blackman, H. Hadavinia, A.J. Kinloch, J.G. Williams, The use of a cohesive zone model to study the fracture of fibre composites and adhesively-bonded joints, International Journal of Fracture 119 (2003) 25-46.

[10] S. Li, M.D. Thouless, A.M. Waas, J.A. Schroeder, P.D. Zavattieri, Mixed-mode cohesive-zone models for fracture of an adhesively bonded polymer-matrix composite, Engineering Fracture Mechanics 73 (2006) 64-78.

[11] V.K. Goyal, E.R. Johnson, V.K. Goyal, Predictive strength-fracture model for composite bonded joints, Composite Structures 82 (2008) 434-446.

[12] ASTM D5528-01, Standard Test Method for Mode I Interlaminar Fracture Toughness of Unidirectional Fiber-Reinforced Polymer Matrix Composites (2007)e1.

[13] J. Schon, A model of fatigue delamination in composites, Composites Science and Technology 60 (1999) 553-558.

[14] N. Blanco, E.K. Gamstedt, L.E. Asp, J. Costa, Mixed-mode delamination growth in carbon-fibre composite laminates under cyclic loading, International Journal of Solids and Structures 41 (2004) 4219-4235.

[15] M.M. Abdel-Wahab, I.A. Ashcroft, A.D. Crocombe, P.A. Smith, Finite element prediction of fatigue crack propagation lifetime in composite bonded joints, Composites Part A: Applied Science and Manufacturing 35 (2004) 213-222.

[16] D.M. Hoyt, S.H. Ward, P.J. Minguet, Strength and Fatigue Life Modelling of Bonded Joints in Composite Structure, Journal of Composites Technology and Research 24 (2002) 190-210.

[17] M. Quaresimin, M. Ricotta, Life prediction of bonded joints in composite materials, International Journal of Fatigue 28(n 10 SPEC. ISS.) (2006) 1166-1176.

Published in International Journal of Fatigue 2010, 32(11), Pages 1774–1787
DOI: 10.1016/j.ijfatigue.2010.04.006

[18] L.R. Deobald, G.E. Mabson, B. Dopker, D.M. Hoyt, J. Baylor, D. Graesser, Interlaminar Fatigue Elements for Crack Growth Based On Virtual Crack Closure Technique, 48th AIAA/ASME/ASCE/AHS/ASC Structures, Structural Dynamics, and Materials Conference, 23 - 26 April 2007, Honolulu, Hawaii.

[19] L.R. Deobald, G.E. Mabson, B. Dopker, D.M. Hoyt, J. Baylor, D. Graesser, Fracture Interface Elements for Static and Fatigue Analysis, ICCM - 16th International Conference on Composite Materials, 8th -13th July 2007, Kyoto, Japan.

[20] B. Yang, S. Mall, K.A. Ravi-Chandar, A cohesive zone model for fatigue crack growth in quasibrittle materials, International Journal of Solids and Structures 38 (2001) 3927-3944.

[21] O. Nguyen, E.A. Repetto, M. Ortiz, R.A. Radovitzky, A cohesive model of fatigue crack growth, International Journal of Fracture 110 (2001) 351-369.

[22] K.L. Roe, T. Siegmund, An irreversible cohesive zone model for interface fatigue crack growth simulation, Engineering Fracture Mechanics 70 (2003) 209-232.

[23] P. Robinson, U. Galvanetto, D. Tumino, G. Belluci, Numerical simulation of fatigue-driven delamination using interface elements, International Journal for Numerical Methods in Engineering 63 (2004) 1824-1848.

[24] D. Tumino, F. Cappello, Simulation of Fatigue Delamination Growth in Composites with Different Mode Mixtures, Journal of Composite Materials 41 (2007) 2415-2441.

[25] A. Turon, J. Costa, P.P. Camanho, C.G. Davila, Simulation of delamination in composites under high-cycle fatigue, Composites Part A: Applied Science and Manufacturing 38 (2007) 2270-2282.

[26] A. Turon, J. Costa, P.P. Camanho, P. Maimi, Simulation of Delamination Onset and Propagation under Fatigue Loading using Cohesive Zone Models, ECCOMAS Thematic Conference on Mechanical Response of Composites, 12-14th September 2007, Porto, Portugal.

[27] T. Ireman, J.C. Thesken, E. Greenhalgh, R. Sharp, M. Gadke, S. Maison, Y. Ousset, F. Roudolff, A. La Barbera, Damage propagation in composite structural elements – coupon experiments and analyses, Composite Structures 36 (1996) 209-220.

[28] P. Harper, S.R. Hallett, Cohesive zone length in numerical simulations of composite delamination, Engineering Fracture Mechanics 75 (2008) 4774-4792.

[29] A. Turon, J. Costa, P. Camanho, P. Maimi, Analytical and Numerical Investigation of the Length of the Cohesive Zone in Delaminated Composite Materials, in: P.P. Camanho, C.G. Dávila, S.T. Pinho, J.J.C. Remmers (Eds.), Mechanical Response of Composites. Series: Computational Methods in Applied Sciences , Vol. 10, 2008, pp. 77-98.

[30] X. Li, S.R. Hallett, M.R.Wisnom, Predicting the effect of through-thickness compressive stress on delamination using interface elements, Composites Part A: Applied Science and Manufacturing 39 (2008) 218-230

[31] J.C. Brewer, P.A. Lagace, Quadratic stress criterion for initiation of delamination, Journal of Composite Materials 22 (1988) 1141-1155.

[32] W. Cui, M.R. Wisnom, M. Jones, A comparison of failure criteria to predict delamination of uni-directional Glass/Epoxy specimens waisted through the thickness, Composites 23 (1992) 158-166.

[33] M.A. Jiménez, A. Miravete, Application of the finite-element method to predict the onset of delamination growth, Journal of Composite Materials 38 (2004) 1309–1335.

[34] M. Juntti, L.E. Asp, R. Olsson, Assessment of evaluation methods for mixed mode bending test, Journal of Composites Technology and Research 21(1) (1992) 37-48.

[35] C. Shet, N. Chandra, Effect of the Shape of traction-displacement cohesive zone curves on the fracture response, Mechanics of Advanced Materials and Structures 11 (2004) 249-275.

[36] B. Cox, Q. Yang, In Quest of Virtual Tests for Structural Composites, Science 314 (2006) 1102-1107

[37] B. Cox, Q. Yang, Cohesive Models for damage evolution in laminated composites, International Journal of Fracture 133 (2005) 107-137.

Published in International Journal of Fatigue 2010, 32(11), Pages 1774–1787
DOI: 10.1016/j.ijfatigue.2010.04.006

[38] A. Turon, C.G. Davila, P.P. Camanho, J. Costa, An engineering solution for mesh size effects in the simulation of delamination using cohesive zone models, Engineering Fracture Mechanics 74 (2007) 1665-1682.

[39] P. Harper, S.R. Hallett, The Influence of Input Parameters on Cohesive Zone Interface Element Models. To be submitted.

[40] J.R. Reeder, K. Demarco, K.S. Whitley, The use of doubler reinforcement in delamination toughness testing, Composites Part A: Applied Science and Manufacturing 35 (2004) 1337-1344.

[41] T. Siegmund, A numerical study of transient fatigue crack growth by use of an irreversible cohesive zone model, International Journal of Fatigue 26 (2004) 929-39.

[42] L.E. Asp, A. Sjogren, E.S. Greenhalgh, Delamination Growth and Thresholds in a Carbon/Epoxy Composite Under Fatigue Loading, Journal of Composites Technology and Research 23 (2001) 55-68.

[43] R. Borg, L. Nilsson, K. Simonsson, Simulating DCB, ENF and MMB experiments using shell elements and a cohesive zone model, Composites Science and Technology 64 (2004) 269-278.